FULL PAPER

Dalton
www.rsc.org/dalton

The structure and dynamic behaviour of disubstituted derivatives of $[Rh_6(CO)_{16}]$ containing heterobidentate bridging phosphine ligands

Elena V. Grachova,[a] Matti Haukka,[b] Brian T. Heaton,*[c] Ebbe Nordlander,[d] Tapani A. Pakkanen,[b] Ivan S. Podkorytov[e] and Sergey P. Tunik*[a]

[a] *St. Petersburg University, Department of Chemistry, Universitetskii pr., 26, St. Petersburg, 198504, Russia*

[b] *Department of Chemistry, University of Joensuu, P.O. Box 111, FIN-80101 Joensuu, Finland*

[c] *Department of Chemistry, University of Liverpool, P.O. Box 147, Liverpool, UK L69 7ZD*

[d] *Inorganic Chemistry 1, Chemical Center, Lund University, Box 124, SE-22100, Lund, Sweden*

[e] *S.V. Lebedev Central Synthetic Rubber Research Institute, Gapsalskaya 1, St. Petersburg, 198035, Russia*

Received 28th November 2002, Accepted 23rd April 2003
First published as an Advance Article on the web 13th May 2003

The solution structures and dynamic behaviour of $[Rh_6(CO)_{14}(\mu\text{-PX})]$ [PX = diphenyl(2-pyridyl)phosphine, (PN); diphenyl(2-thienyl)phosphine, (PS); diphenyl(vinyl)phosphine, (PV)] have been studied by multinuclear NMR and the X-ray structure of $[Rh_6(CO)_{14}(\mu,\kappa^3\text{-PV})]$ is reported. In solution, the above clusters undergo a variety of localised CO-exchanges and the mechanisms of these are discussed. The PV ligand in $[Rh_6(CO)_{14}(\mu,\kappa^3\text{-PV})]$ is hemilabile and exhibits facile exchange/reorientation of the vinyl group.

Introduction

In recent years, we have carried out systematic studies on the solid state [1–3] and solution structures,[4] reactivity [5,6] and dynamic properties [7] of substituted derivatives of $[Rh_6(CO)_{16}]$. It has been found that incorporation of one monodentate hetero-ligand into the coordination sphere of the parent cluster significantly changes the dynamic behaviour of the carbonyl ligands.[4,7,8] It has been shown that the dynamics of the lowest energy CO-exchange process in $[Rh_6(CO)_{15}(PR_3)]$ can be described as exchange of terminal (CO_t) and face-bridging (CO_{fb}) carbonyls, which are associated with the *substituted* rhodium atom, with concomitant exchange of the phosphine between the two terminal sites on the same rhodium atom. For $[Rh_6(CO)_{14}(\mu,\kappa^2\text{-PP})]$, which contain a bridging diphosphine ligand, the exchange of carbonyls about the substituted rhodium atoms is completely suppressed because, unlike the monodentate phosphine in $[Rh_6(CO)_{15}(PR_3)]$, the phosphorus atoms in the bridging diphosphine ligand cannot exchange sites to allow a similar CO-migration on the substituted Rh-atoms.[8] For $[Rh_6(CO)_{14}(\mu,\kappa^2\text{-PP})]$, the lowest energy CO-exchanges involve the ***u***nsubstituted rhodium atoms (U-type dynamics) and these CO-exchanges have been rationalized on the basis of a turn-style rotation of three carbonyl ligands (one is a face bridging CO) around the corresponding rhodium centre. When PP = dppe ($Ph_2PCH_2CH_2PPh_2$) or dppe[f] ($(C_6F_5)_2PCH_2CH_2P(C_6F_5)_2$, an additional very low energy dynamic process is observed; this involves the oscillation of the ligand backbone and the rate of this depends strongly on the intramolecular van der Waals interaction between the phosphorus substituents and adjacent carbonyl ligands. As an extension of these investigations, we have studied the dynamic properties of the hetero-bidentate ligand disubstituted clusters, $[Rh_6(CO)_{14}(\mu\text{-PX})]$ [PX = diphenyl(2-pyridyl)phosphine, (PN); diphenyl(2-thienyl)phosphine, (PS); diphenylvinylphosphine, (PV)]. The CO-stereochemical nonrigidity, together with the hemilability of the diphenylvinyl phosphine ligand, have been studied using ^1H and ^{13}C EXSY NMR spectroscopy. The solid state structure of $[Rh_6(CO)_{14}(\mu,\kappa^3\text{-PV})]$ has been established using X-ray crystallography and the solution structures of all three substituted clusters (PX = PN, PS, PV) have been elucidated by means of ^{13}C-{^{103}Rh} and ^{31}P-{^{103}Rh} HMQC techniques.

Experimental

General

All solvents – dichloromethane, chloroform, acetonitrile, hexane and diethyl ether (Merck; Vekton) – were distilled over appropriate drying agents under an atmosphere of nitrogen before use. $[Rh_6(CO)_{14}(\mu,\kappa^2\text{-PS})]$ **1**, $[Rh_6(CO)_{14}(\mu,\kappa^2\text{-PN})]$ **2** and $[Rh_6(CO)_{14}(\mu,\kappa^3\text{-PV})]$ **3** were synthesized according to published procedures.[9] Single crystals of **3** suitable for X-ray analysis were obtained from a mixture of chloroform/heptane at +3 °C.

NMR measurements

^1H, ^{13}C, ^{31}P, ^{13}C-{^{103}Rh}, ^{31}P-{^{103}Rh} HMQC NMR and ^{13}C EXSY spectra were recorded on DPX-300, Bruker AM200WB, AMX400 and Bruker AM-500 instruments. HMQC and EXSY measurements were carried out as described previously.[7,10]

X-Ray crystallography

X-Ray diffraction data were collected with a Nonius Kappa CCD diffractometer using Mo-Kα radiation (λ = 0.71073 Å) and the Collect [11] data collection program. The Denzo/Scalepack [12] programs were used for cell refinements and data reduction. The structure of **3** was solved by the Patterson method using the DIRDIF-99 [13] and WinGX [14] graphical user interface. A multi-scan absorption correction, based on equivalent reflections (XPREP in SHELXTL v. 5.1),[15] was applied to **3** (T_{max}/T_{min} was 0.27606/0.22522). The structure was refined using SHELXL97.[16] All hydrogens atoms in **3** were constrained to ride on their parent atom. Crystallographic data are summarized in Table 1. Selected bond lengths and angles are shown in Table 2 and the molecular structure in Fig. 1.

CCDC reference number 198809.

See http://www.rsc.org/suppdata/dt/b2/b211790h/ for crystallographic data in CIF or other electronic format.

Results and discusion

Molecular structure of $[Rh_6(CO)14(\mu,\kappa^3\text{-PV})]$, 3

The solid state structures of $[Rh_6(CO)_{14}(\mu,\kappa^2\text{-PS})]$ (**1**) and $[Rh_6(CO)_{14}(\mu,\kappa^2\text{-PN})]$ (**2**), have been determined (see preceding

DOI: 10.1039/b211790h

Table 1 Crystallographic data for $[Rh_6(CO)_{14}(\mu,\kappa^3\text{-}Ph_2PCH{=}CH_2)]$, **3**

	3
Empirical formula	$C_{28}H_{13}O_{14}PRh_6$
M_w	1221.81
Crystal system	Monoclinic
Space group	$P2_1/c$
λ/Å	0.71073
a/Å	15.1678(3)
b/Å	10.8998(2)
c/Å	20.6922(5)
β/°	90.125(1)
V/Å^3	3420.95(12)
T/K	150(2)
Z	4
D_c/gcm^{-3}	2.372
μ/mm^{-1}	2.939
No. refl. collected	28609
No. unique refl.	7792
R_{int}	0.0476
$R1$ [a] ($I \geq 2\sigma$)	0.0308
$wR2$ [b] ($I \geq 2\ \sigma$)	0.0533

[a] $R1 = \Sigma||F_o| - |F_c||/\Sigma|F_o|$. [b] $wR2 = [\Sigma[w(F_o^2 - F_c^2)^2]/\Sigma[w(F_o^2)^2]]^{1/2}$.

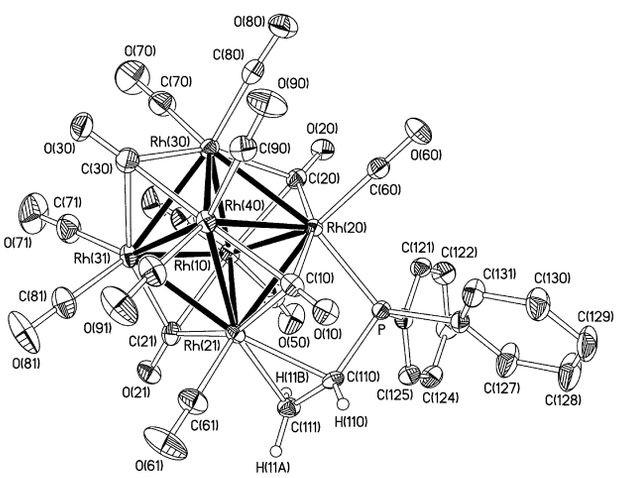

Fig. 1 ORTEP view of $[Rh_6(CO)_{14}(\mu,\kappa^3\text{-}Ph_2PCH{=}CH_2)]$, **3**, probability level 50%.

paper)[9] and in each case the PX ligands are coordinated through both phosphorus and X (X = S or N) such that PX occupies two terminal sites on adjacent atoms of the rhodium octahedron and the carbonyls (ten terminal and four face bridging) occupy the remaining sites, similar to those found in the parent $[Rh_6(CO)_{16}]$ cluster. The solid state structure of $[Rh_6(CO)_{14}(\mu,\kappa^3\text{-PV})]$ (**3**) has been established in the present work using X-ray crystallography (see Fig. 1) and selected structural parameters are given in Table 2. The numbering scheme for the rhodium atoms and CO ligands shown in Fig. 1 have also been used for **1** and **2** in the discussion of their solution structures and stereochemical nonrigidity.

The bidentate diphenylvinylphosphine ligand in **3** is coordinated to the Rh_6-octahedron through the phosphorus atom and the vinyl double bond to form a bridge between two adjacent rhodium atoms, as suggested earlier on the basis of spectroscopic data.[9] This coordination mode of the $Ph_2PCH{=}CH_2$ ligand has also been found in disubstituted derivatives of Os_3[17] and Co_3C[18] clusters; the analogous diphenylallylphosphine, $Ph_2PCH_2CH{=}CH_2$, also exhibits a similar bridging mode of coordination through both the phosphorus and the double bond in the related $[Rh_6(CO)_{16}]$ derivative.[19] The principal bond lengths and averages for **3** fall in the range found for related clusters.[8,9,20] However, there are some structural differences for **3** when compared to related analogues. In the solid state, the vinyl fragment in **3** adopts a conformation in which

Table 2 Selected bond lengths (Å) in $[Rh_6(CO)_{14}(\mu,\kappa^3\text{–}Ph_2PCH{=}CH_2)]$, **3**. For numbering scheme, see Fig. 1

Rh–Rh	
Rh(10)–Rh(20)	2.7953(4)
Rh(10)–Rh(21)	2.7861(4)
Rh(10)–Rh(30)	2.7675(4)
Rh(10)–Rh(31)	2.7389(5)
Rh(20)–Rh(21)	2.7021(4)
Rh(30)–Rh(31)	2.7861(5)
Rh(20)–Rh(30)	2.7603(4)
Rh(21)–Rh(31)	2.7549(4)
Rh(40)–Rh(30)	2.7215(4)
Rh(40)–Rh(31)	2.7379(4)
Rh(40)–Rh(20)	2.7932(4)
Rh(40)–Rh(21)	2.8311(4)
Average [a]	**2.7646(361)**
Rh–μ_3-CO	
Rh(40)–C(10)	2.078(4)
Rh(20)–C(10)	2.229(4)
Rh(21)–C(10)	2.282(4)
Rh(10)–C(20)	2.196(4)
Rh(20)–C(20)	2.087(4)
Rh(30)–C(20)	2.332(4)
Rh(10)–C(21)	2.204(4)
Rh(21)–C(21)	2.138(4)
Rh(31)–C(21)	2.204(4)
Rh(40)–C(30)	2.189(4)
Rh(30)–C(30)	2.138(4)
Rh(31)–C(30)	2.267(4)
Average [a]	**2.195(76)**
Rh–t-CO	
Rh(10)–C(40)	1.896(4)
Rh(10)–C(50)	1.917(4)
Rh(20)–C(60)	1.887(5)
Rh(21)–C(61)	1.901(5)
Rh(30)–C(70)	1.902(4)
Rh(31)–C(71)	1.901(4)
Rh(30)–C(80)	1.907(5)
Rh(31)–C(81)	1.900(5)
Rh(40)–C(90)	1.916(4)
Rh(40)–C(91)	1.919(4)
Average [a]	**1.905(10)**
Rh–L	
Rh(20)–P	2.2766(9)
Rh(21)–C(110)	2.239(4)
Rh(21)–C(111)	2.214(4)

[a] Values of variance $S = [(x_i - \bar{x})^2/(n-1)]^{1/2}$ for the averages are given in parentheses.

the α-hydrogen lies outside the Rh(10)Rh(20)Rh(21) triangle; this presumably occurs because it minimises the nonbonding contacts between the vinyl moiety and C(50)O. This disposition of the rigid P–CH=CH_2 bridge results in the close approach of the vinyl α-hydrogen (H(110)) and the bridging C(10)O ligand which makes the corresponding nonbonded C(110)–C(10) and H(110)–C(10) contacts (2.891 and 2.883 Å, respectively) rather short. The repulsion between the C(10)O ligand and the vinyl fragment results in a shift of the face-bridging C(10)O towards the Rh(40) vertex of the octahedron. This kind of structural distortion of the face-bridging CO is very unusual for phosphine substituted derivatives of $[Rh_6(CO)_{16}]$, where normally the face-bridging carbonyl is shifted towards the phosphine substituted rhodium atom(s). For $[Rh_6(CO)_{14}(\mu,\kappa^3\text{-}Ph_2P\text{-}(allyl))]$,[19] the phosphine coordination on the Rh_6 octahedron is similar to that found in **3**. However, the more flexible P–CH_2–CH=CH_2 chain of the allyl fragment allows a shift of the

Table 3 ^{13}C, ^{31}P, ^{103}Rh NMR data for $[Rh_6(CO)_{14}(\mu,\kappa^n\text{-PX})]$ (PX = PS, n = 2, **1**; PN, n = 2, **2** PV, n = 3, **3**). For numbering scheme, see Fig. 1

	1 (298 K, $CDCl_3$)			**2** (298 K, $CDCl_3$)			**3** (180 K, CD_2Cl_2)		
Assignment[a]	δ (^{13}C)[b]	$^1J_{Rh-C}$	Other SSCCs	$\delta(^{13}C)$[b]	$^1J_{Rh-C}$	Other SSCCs	$\delta(^{13}C)$[b,c]	$^1J_{Rh-C}$	Other SSCCs
C(10)O	240.6	24; 36		251.5	18; 27; 31		238.5		
C(20)O	239.4	20; 31		240.9	19; 30		239.2		
C(21)O	247.1	27		247.7	24; 36		235.6	29	
C(30)O	231.1	27		232.6	26		232.7	28	
C(40)O	182.8	69		184.5	70		181.9	71	
C(50)O	181.0	65		182.7	67		180.3	67	
C(60)O	184.5	69	$^2J_{P-C}$ = 10	186.0	67	$^2J_{P-C}$ = 5	187.9	74	
C(61)O	182.2	68		182.3	69		183.5	71	
C(70)O	180.7	68	$^3J_{P-C}$ = 25	184.1	70	$^3J_{P-C}$ = 24	183.2	69	$^3J_{P-C}$ = 17
C(71)O	180.5	70		181.5	68		181.6	69	
C(80)O	180.8	67		184.3	69		181.9	71	
C(81)O	180.2	70	$^nJ_{P-C}$ = 4	180.0	69		181.9	71	
C(90)O	183.8	70		179.4	69		181.0	69	
C(91)O	183.5	67	$^3J_{P-C}$ = 23	180.9	70	$^3J_{P-C}$ = 20	181.7	69	$^3J_{P-C}$ = 19
	$\delta(^{31}P)$	$^1J_{Rh-P}$		$\delta(^{31}P)$	$^1J_{Rh-P}$		$\delta(^{31}P)$	$^1J_{Rh-P}$	
P	14.3	140		26.2	143		18.6	125	
	$\delta(^{103}Rh)$			$\delta(^{103}Rh)$			$\delta(^{103}Rh)$	$\delta(^{103}Rh)$ (298 K)[d]	
Rh(10)	−400			−450			−335	−288	
Rh(20)	−350			−410			−430	−383	
Rh(21)	+15			+650			−265	−218	
Rh(30)	−385			−370			−265	−218	
Rh(31)	−330			−415			−325	−278	
Rh(40)	−355			−315			−495	−448	

[a] Assignments can be reversed for the following resonances: C(40)O/C(50)O. [b] Assignments can be reversed for the following resonances: C(71)O/C(81)O. [c] Assignments can be reversed for the following resonances: C(61)O/C(90)O. [d] The values of $\delta(^{103}Rh)$ have been adjusted to room temperature using the following gradient value +0.4 ppm/+1 K.

adjacent face-bridging carbonyl, C(10)O, towards Rh(20) and Rh(21); this is the normal displacement induced by electronic effects of the substituting heteroligand.[3]

Solution structure and dynamics in 1–3

The NMR data for **1**–**3**, together with the assignments of the resonances, are given in Table 3; the assignments are based on ^{13}C-{^{103}Rh} and ^{31}P-{^{103}Rh} HMQC measurements using previously described procedures.[7] The number of resonances in the ^{13}C, ^{31}P, ^{103}Rh spectra and their multiplicity clearly points to retention of the solid state structures in solution. In accordance with the completely asymmetric structures of **1**–**3** in the solid state, the low temperature ^{13}C and ^{103}Rh spectra contain fourteen carbonyl and six rhodium resonances (see Table 3). The chemical shifts of the rhodium nuclei bonded to phosphorus and carbon atoms in these clusters fall in the range −218 to −450 ppm, which is similar to data obtained earlier for related phosphorus donor derivatives;[8] these values should be compared to the values of the rhodium chemical shifts when bonded to sulfur and nitrogen in **1** and **2**, which are found to be at substantially lower field (+15 and +650 ppm, respectively). This illustrates the sensitivity of the rhodium chemical shifts to the nature of adjacent ligands and the shifts of these latter resonances are in-keeping with the low field shift found for the Rh–($NCCH_3$) resonance in the monoacetonitrile substituted cluster, $[Rh_6(CO)_{15}(NCCH_3)]$ (+470 ppm).[7] The values of the ^{13}C chemical shifts and the ^{103}Rh–^{13}C, ^{31}P–^{13}C, coupling constants found for **1**–**3** do not display any irregularities when compared with the other substituted $[Rh_6(CO)_{16}]$ derivatives.[4,7,8]

Above the low temperature limiting spectra, the ligands in **1**–**3** start to take part in a variety of different dynamic processes (see Table 4). In **1** and **2**, the onset of CO-exchange is observed at 320 and 300 K, respectively; in both clusters, only the carbonyls associated with the non-phosphorus-substituted Rh atoms are involved in exchange (*U*-type dynamics).[7,8] In contrast to the rather rigid nature of **1** and **2**, which show a similar behaviour to the $[Rh_6(CO)_{16}]$ derivatives containing bridging diphosphines,[8] the carbonyls on the the non-phosphorus-substituted Rh atoms in **3** start to undergo *U*-type exchange at about 210 K and, in addition to these carbonyl exchanges, the vinyl group also undergoes rearrangement in the temperature range 273–343 K.

Both the temperatures required to induce the CO-exchanges in **1** and **2** and the COs involved in these exchanges are somewhat similar to those found in the diphosphine-substituted clusters.[8] Thus, the face-bridging ligand, C(30)O, is involved in exchange with adjacent terminal carbonyls, whereas the similar face-bridging carbonyl, C(10)O, is *not*. An important difference in the dynamic behaviour of **1** and **2** when compared to that found for $[Rh_6(CO)_{14}(\mu,\kappa^2\text{-PP})]$ is the different exchange behaviour of the face-bridging carbonyls, C(20)O and C(21)O. For the diphosphine derivatives,[8] both these face-bridging COs are involved in exchange with the terminal carbonyls, C(40)O and C(50)O, whereas for **1** and **2** only exchange of C(21)O↔C(40)O,C(50)O is observed; C(20) is *not* involved in exchange. It is interesting to note that this CO-exchange occurs on the surface of the octahedron, which is adjacent to the nitrogen or sulfur donor atoms and opposite/remote from the phosphorus. Nevertheless, we believe that this exchange stems from activation by the phosphorus because:

(a) the temperature of the onset of this exchange is similar to that observed for the other diphosphine derivatives,[8]

(b) the data obtained for the monosubstituted clusters, $[Rh_6(CO)_{15}L]$,[7] clearly show that when L = PR_3 this *U*-type of CO-exchange occurs at temperatures *ca.* 20–30 °C lower when compared with analogous clusters where L ≠ PR_3. Moreover, a preliminary study on $[Rh_6(CO)_{15}(pyridine)]$ shows that there is *no* CO-exchange below 320 K.[21] These observations suggest

Table 4 The carbonyl ligands involved in the lowest energy dynamics in $[Rh_6(CO)_{14}(\mu,\kappa^n\text{-PX})]$ (PX = PS, n = 2, **1**; PN, n = 2, **2** PV, n = 3, **3**). For numbering scheme, see Fig. 1

1	**2**	**3**	
320 K, τ_{mix} = 0.1 s	300 K, τ_{mix} = 0.1 s	230 K, τ_{mix} = 0.1 s	298 K, τ_{mix} = 0.1 s
		10 ↔ 90, 91	10 ↔ 90, 91
		90 ↔ 91	90 ↔ 91
			20 ↔ 40, 50
21 ↔ 40, 50	21 ↔ 40, 50		21 ↔ 40, 50
40 ↔ 50	40 ↔ 50		40 ↔ 50
30 ↔ 70, 80	30 ↔ 70, 80		
70 ↔ 80	70 ↔ 80		
30 ↔ 71, 81	30 ↔ 71, 81		
71 ↔ 81	71 ↔ 81		
30 ↔ 90, 91			
90 ↔ 91			

that there is a *long range* regioselectivity of the carbonyl scrambling induced by the coordinated phosphine.

The onset of the CO exchange in **3** starts at a very low temperature (see Table 4) when compared with all other $[Rh_6(CO)_{16-x}L_x]$ clusters studied earlier.[7,8] Furthermore, the carbonyls involved in exchange in **3** (C(10)O↔C(90)O,C(91)O) are *not* involved in any dynamic process in any of the other $[Rh_6(CO)_{14}(\mu\text{-PX})]$ derivatives over the temperature range studied. From a consideration of ground state properties (structural and spectroscopic data), we feel that the important contributory factor for this exchange in **3** is the structural distortion of the face-bridging C(10)O ligand referred to above. The displacement of C(10)O in **3** towards Rh(40) makes the C(10)–Rh(40) bond length the shortest Rh–μ_3-CO distance both in the series of disubstituted clusters studied earlier[8] and in the present paper. This, in turn, makes the ground state of the {Rh(40);C(10)O;C(90)O;C(91)O} fragment "preprepared" for the transformation into a tris-terminal CO configuration to allow facile turnstile rotation (TSR) of these COs and is probably one of the key points in promoting this particular exchange. At higher temperatures, exchange of both face-bridging carbonyls, C(20)O and C(21)O, with two terminal carbonyls, C(40)O and C(50)O, occurs in **3**, but the face-bridging carbonyl, C(30)O, is *not* involved in any exchange, unlike the behaviour found in **1** and **2**. It is also interesting to note that in **1**–**3**, of the two possibilities for the face-bridging carbonyls, C(20)O and C(21)O, to take part in the TSR scrambling about Rh(10) or Rh(30), the preferred exchange involves Rh(10), which has a shorter contact with C(20)O.

The VT ^{1}H NMR spectra of **3**, (see Fig. 2), show that the bridging P–CH=CH_2 fragment is also involved in a dynamic process, which can be rationalised as involving an equilibrium between two isomeric forms of the bridging ligand on the basis of ^{1}H–^{1}H EXSY measurements (see Fig. 3). Low temperature ^{1}H and ^{31}P NMR spectra show the presence of both isomers in solution, one of which (minor) is thermodynamically unfavourable. At the low temperature limit, there are two duplicate sets of resonances corresponding to the three vinyl protons of the major and minor isomers. Assignment of the resonances has been made on the basis of ^{1}H–^{1}H COSY measurements and the observed values of the coupling constants in the phosphorus bonded vinyl fragment, (see Table 5). Increasing the temperature results in broadening of the resonances due to the minor isomer and they eventually coalesce with the resonances due to the major species. The temperature dependence of this exchange indicates that it is independent of the CO-exchanges. Although it is diifficult to assign the exact stereochemistry of these two isomers, we feel that the most probable isomers, which could be involved in this equilibrium, are shown schematically in Scheme 1, together with the proposed intermediate involved in this isomerisation. These two isomers differ only in

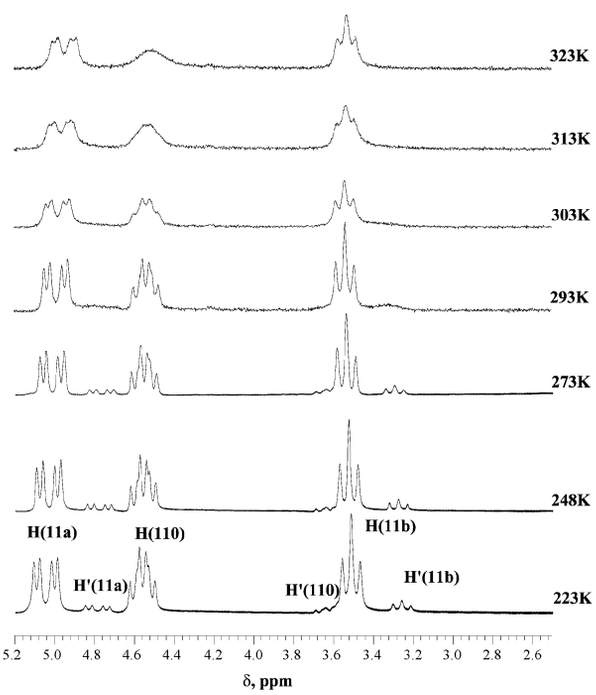

Fig. 2 ^{1}H VT spectra of **3**, $CDCl_3$; H and H′ denote the signals corresponding to the major and minor isomers, respectively.

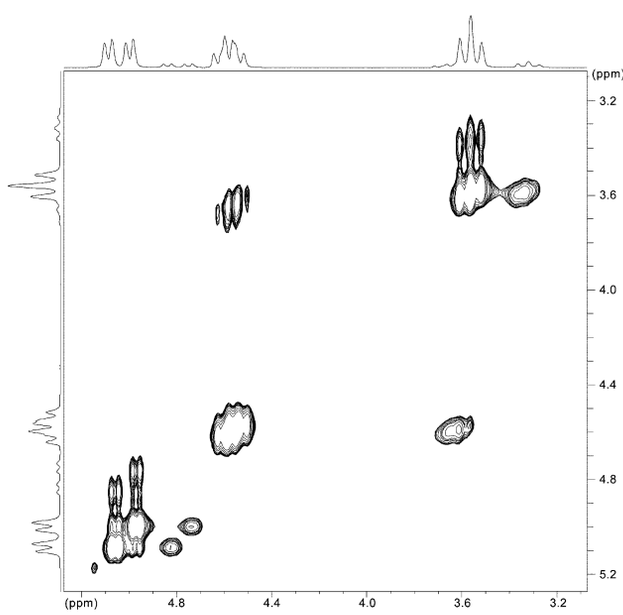

Fig. 3 ^{1}H–^{1}H EXSY NMR spectrum of **3**, 293 K, $CDCl_3$.

Table 5 ^{1}H NMR spectroscopic data for major and minor isomers of **3** at 220 K in $CDCl_3$

	Assignment	δ/ppm	Spin–spin coupling constant/Hz
	Major isomer		
	H(11a)	5.06	^{3}J(P–H(11a)) = 27, ^{3}J(H(11a)–H(110)) = 9, ^{2}J(H(11a)–H(11b)) = 3
	H(110)	4.58	^{2}J(P–H(110)) = 14, ^{3}J(H(110)–H(11a)) = 9, ^{3}J(H(110)–H(11b)) = 14
	H(11b)	3.55	^{3}J(P–H(11b)) = 14, ^{3}J(H(11b)–H(110)) = 14, ^{2}J(H(11b)–H(11a)) = 3
	Minor isomer		
	H(11a)	4.80	^{3}J(P–H(11a)) = 26, ^{3}J(H(11a)–H(110)) = 10
	H(110)	3.65	^{2}J(P–H(110)) = 14, ^{3}J(H(110)–H(11a)) = 10, ^{3}J(H(110)–H(11b)) = 14
	H(11b)	3.30	^{3}J(P–H(11b)) = 14, ^{3}J(H(11b)–H(110)) = 14

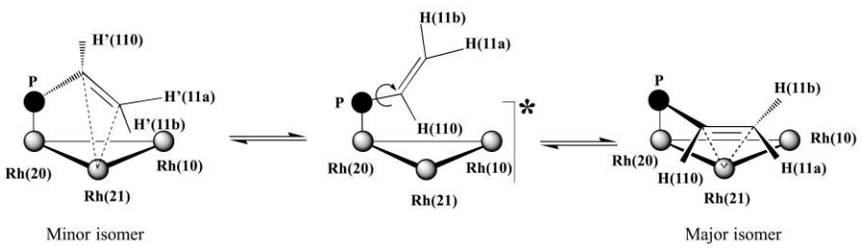

Scheme 1 Equilibrium between the isomers **3** and **3′** in solution (for the sake of simplicity, only the relevant triangle of the rhodium octahedron is shown).

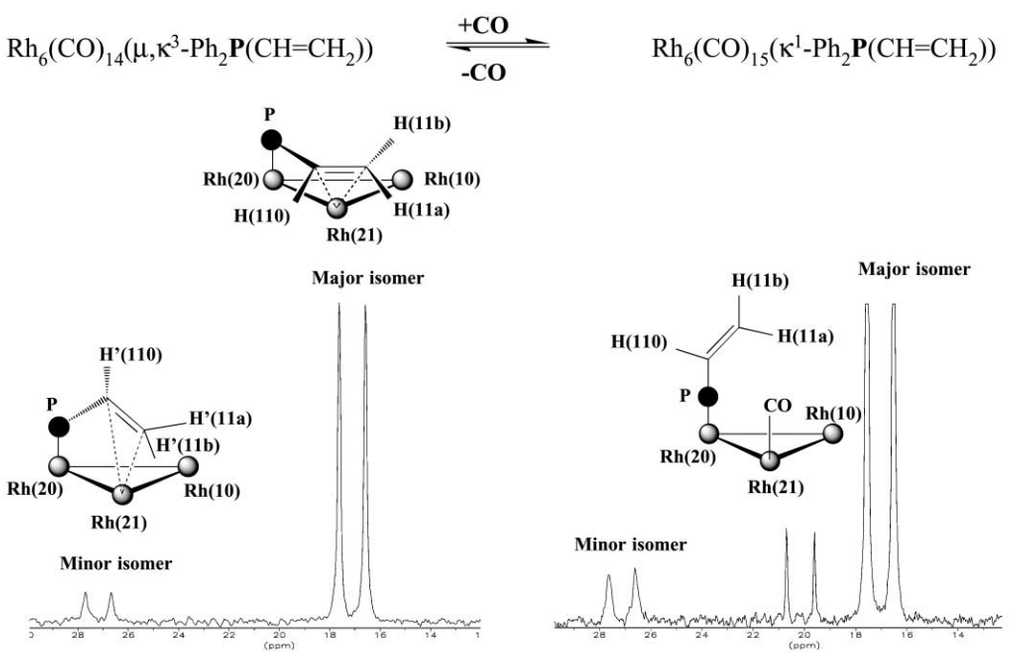

Fig. 4 ^{31}P NMR spectra of **3** at 298 K, in $CDCl_3$, with and without saturation of the solution with gaseous CO, 1 atm.

the orientation of the P–CH=CH_2 fragment with respect to the Rh(20)Rh(21)Rh(40) triangle. We assign the structure of the major isomer to that found in the solid state where intramolecular nonbonding contacts are minimised by the "out of triangle" orientation of α-CH moiety of the vinyl group. This evidently makes this structure less strained and consequently dominant in the equilibrium. The structure proposed for the minor isomer is more sterically hindered due to repulsion between the α-CH moiety and C(50)O which makes this configuration thermodynamically less favourable. Estimation of the standard enthalpy of the isomerization using VT ^{1}H NMR spectra in d^{8}-toluene (223–273 K) showed a very small energy difference between these two isomers, (7 ± 2 kJ mol^{-1}) that is consistent with a slight contribution of nonbonding contacts to distinguish the conformers. The [$Os_3(CO)_{10}$(μ,κ^{3}-Ph_2PCH=CH_2)] cluster,[17] containing a bridging PV ligand, also gives rise to two isomeric forms; these isomers are however much less labile, which allows them to be separated chromatographically. On the basis of their ^{1}H NMR spectra, they have been assigned to isomers involving occupancy of axial/equatorial sites by the phosphorus in the Os_3-triangle. We feel that the isomeric equilibrium observed for **3** is best described by the mechanism shown in Scheme 1. This scheme involves dissociation of the vinyl double bond, rotation of the vinyl fragment about the P–C bond followed by recoordination in a slightly different orientation; this type of rearrangement stems from the hemilability of the vinylphosphine and the ready displacement of the vinyl group is illustrated by the reversible addition of CO to **3**. Thus, the ^{31}P NMR spectra of the isomeric mixture of **3**, *with* and *without* gaseous CO, are shown in Fig. 4. The doublet centered at 20.0 ppm in the spectrum of the CO saturated solution can be unambigously assigned to the monodentate coordinated PV ligand on the basis of data obtained for the reaction of PV with [$Rh_6(CO)_{15}$(NCMe)].[9] The hemilability of this functionalized phosphine, along with the readily reversible reaction with CO, suggests that **3** may be a useful precursor in catalytic

reactions and studies of its catalytic activity in alkene isomerization is now in progress.

Acknowledgements

We are grateful to the EPSRC for financial support for NMR equipment, to the Russian Center for Natural Sciences (grant E-02–5.0–60) and to INTAS (SPT and EVG) for travel support. We also appreciate J. A. Iggo's assistance with the HMQC measurements.

References

1 S. P. Tunik, A. V. Vlasov, N. I. Gorshkov, G. L. Starova, A. B. Nikol'skii, M. I. Rybinskaya, A. S. Batsanov and Y. T. Struchkov, *J. Organomet. Chem.*, 1992, **433**, 189.
2 S. P. Tunik, A. V. Vlasov, K. V. Kogdov, G. L. Starova, A. B. Nikolskii, O. S. Manole and Y. T. Struchkov, *J. Organomet. Chem.*, 1994, **479**, 59.
3 D. H. Farrar, E. V. Grachova, A. Lough, C. Patirana, A. J. Poë and S. P. Tunik, *J. Chem. Soc., Dalton Trans.*, 2001, 2015.
4 S. P. Tunik, I. S. Podkorytov, B. T. Heaton, J. A. Iggo and J. Sampanthar, *J. Organomet. Chem.*, 1998, **550**, 221.
5 S. P. Tunik, A. V. Vlasov, A. B. Nikol'skii, V. V. Kryvikh and M. I. Rybinskaya, *Organomet. Chem.*, 1991, **4**, 286 (in Russian).
6 A. J. Poë and S. P. Tunik, *Inorg. Chim. Acta*, 1998, **268**, 189.
7 E. V. Grachova, B. T. Heaton, J. A. Iggo, I. S. Podkorytov, D. J. Smawfield, S. P. Tunik and R. Whyman, *J. Chem. Soc., Dalton Trans.*, 2001, 3303.
8 D. H. Farrar, E. V. Grachova, M. Haukka, B. T. Heaton, J. A. Iggo, T. A. Pakkanen, I. S. Podkorytov and S. P. Tunik, *Inorg. Chim. Acta*, in press.
9 S. P. Tunik, I. O. Koshevoy, A. J. Poë, D. H. Farrar, E. Nordlander, M. Haukka and T. A. Pakkanen, *Dalton Trans.*, 2003, DOI: 10.1039/b300951c.
10 F. M. Dolgushin, E. V. Grachova, B. T. Heaton, J. A. Iggo, I. O. Koshevoy, I. S. Podkorytov, D. J. Smawfield, S. P. Tunik, R. Whyman and A. I. Yanovskii, *J. Chem. Soc., Dalton Trans.*, 1999, 1609.
11 Collect data collection software, Nonius B.V., Delft, The Netherlands, 1997–2000.
12 Z. Otwinowski and W. Minor, *Processing of X-ray Diffraction Data Collected in Oscillation Mode*, in *Methods in Enzymology, Volume 276, Macromolecular Crystallography, Part A*, ed. C. W. Carter Jr. and R. M. Sweet, Academic Press, New York, 1997, pp. 307–326.
13 P. T. Beurskens, G. Beurskens, R. de Gelder, S. Garcia-Granda, R. O. Gould, R. Israel and J. M. M. Smits, in The DIRDIF-99 program system, The Netherlands, 1999.
14 L. J. Farrugia, *J. Appl. Crystallogr.*, 1999, **32**, 837.
15 G. M. Sheldrick, in SHELXTL Version 5.1, Madison, WI, USA, 1998.
16 G. M. Sheldrick, SHELXL-97, Program for refinement of crystal structures, University of Göttingen, Germany, 1997; G. M. Sheldrick, in SHELXL97, Program for Crystal Structure Refinement, 1997.
17 R. Giordano, E. Sappa, G. Predieri and A. Tiripicchio, *J. Organomet. Chem.*, 1997, **547**, 49.
18 G. A. Acum, M. J. Mays, P. R. Raithby and G. A. Solan, *J. Organomet. Chem.*, 1996, **508**, 137.
19 S. I. Pomogailo, I. I. Chuev, G. I. Dzhardimalieva, A. V. Yarmolenko, V. D. Makhaev, S. M. Aldoshin and A. D. Pomogailo, *Russ. Chem. Bull.*, 1999, **6**, 1185.
20 C. Babij, C. S. Browning, D. Farrar, I. O. Koshevoy, I. S. Podkorytov, A. J. Poë and S. P. Tunik, *J. Am. Chem. Soc.*, 2002, **124**, 8922.
21 S. P. Tunik, E. V. Grachova, unpublished results.